Journal of Statistical Physics, Vol. 69, Nos. 1/2, 1992

Scaling Relationships for Anisotropic Random Walks

A. H. Gandjbakhche,[1] R. F. Bonner,[1] and R. Nossal[1]

Received September 6, 1991; final April 9, 1992

Aspects of transport in a highly multiple-scattering environment are investigated by examining random walkers moving in media having anisotropic angular scattering cross sections (turn-angle distributions). A general expression is obtained for the mean square displacement $\langle x^2 \rangle$ of a random walker executing an n-step walk in an infinite homogeneous material, and results are used to predict scaling relations for the probability $\gamma(\rho)$ that a walker returns to the planar surface of a semi-infinite medium at a distance ρ from the point of its insertion.

KEY WORDS: Anisotropic random walks; multiple scattering; scaling relations.

1. INTRODUCTION

A number of remote sensing procedures have been developed which involve the multiple scattering of an applied radiation field as it propagates through a randomly structured medium. Typically, the probe radiation is inserted at one location on the surface of a material and detected at a surface somewhat distant from the point of incidence. Examples are LIDAR (light detection and ranging) of the atmosphere and oceans,[1–4] seismographic procedures involving the propagation of sound waves,[5] pressure-transient analyses of fluid-filled reservoirs,[6] and various optical methods for medical diagnosis.[7–10] These techniques involve the migration of localized packets of energy, which can be described by diffusion or random walk models.

[1] National Institutes of Health, Bethesda, Maryland 20892.

0022-4715/92/1000-0035$06.50/0 © 1992 Plenum Publishing Corporation

Our own interests involve models of light propagation through biological tissue.[11–14] We are particularly interested in quantities related to measurements of photon intensities and path lengths. Although the angular scattering cross sections of tissue are strongly peaked in the forward direction, isotropic diffusion models frequently can be used to analyze experimental observations as long as suitably modified, "transport-corrected" absorption and scattering coefficients are employed. In this paper we discuss aspects of such anisotropic scattering, one purpose being to derive scaling relationships for surface emission profiles and thereby infer how equivalent transport cross sections should be defined. We verify our theoretical results by comparison with the outcome of related Monte Carlo simulations. Because we ignore the effects of absorption, the model herein discussed is but an incomplete representation of the diffusion of light in optically turbid media. Scaling relations for photon transport, for a model which includes absorption, are discussed in a companion paper.[15]

We specifically examine the behavior of random walkers inserted into, and then moving within, a semi-infinite homogeneous scattering medium bounded by a planar surface. We show, in this paper and ref. 15, that several parameters of surface-reemitted photons can be scaled by functions of the mean cosine of the polar scattering angle $g = \langle \cos \theta \rangle$. We compute quantities such as $P(n)$, which is the distribution of the number of steps n needed to return to the surface, and $\gamma(\rho)$, which is the probability density of walkers reemitted on the surface at a distance ρ from the point of insertion. Particular emphasis is given to describing short pathlength random walks, for which several run-length (i.e., scattering-length) distributions are investigated. We find that $P(n)$ is a functional of $n^* \equiv h(g) \cdot n$, where $h(g) = (1 - g)/(1 + g)$ seems to be a suitable factor for fitting data at small and intermediate values of n^*. The distribution $\gamma(\rho)$ correspondingly can be written as a functional of a reduced variable as $\rho^* \equiv s(g) \cdot \rho$, where ρ is the distance expressed in terms of root mean square run lengths. However, the function $s(g)$ generally depends on the explicit form of the run-length distribution: for example, if the run length (distance between turns or collisions) is exponentially distributed, we find that the relevant functional dependence for short pathlengths is $\rho^* = [(1 - g)/(1 + g)^{1/2}]\rho$. We show that, for any given scattering-length distribution, the scaling of $\gamma(\rho)$ can be expressed in terms of a similarity transformation involving the mean square displacement of a random walker moving in an infinite medium.

In Section 2 we first derive a general expression for the mean square displacement $\langle x^2 \rangle$ and show how this quantity varies with the scattering-length distribution. We next show, in Section 3, how the similarity transformation can be used to predict the scaling of the surface intensities.

In Section 4 we describe the Monte Carlo simulations and present results which substantiate the theoretical inferences. We also explicitly demonstrate that scaled results for anisotropic scattering can be represented by our previously derived equivalent analytic theory of photon migration in isotropic media.[11] A short discussion appears in Section 5, and the proof of some analytical results is described in the Appendix.

2. RANDOM FLIGHT IN AN INFINITE MEDIUM

We here consider a random walk in a homogeneous medium, for simplicity first deriving relationships in planar geometry and then generalizing to three dimensions. Throughout the remainder of the paper, we use the terminology "walker" and "photon" interchangeably.

Consider a track in two dimensions, characterized by length variables $\{l\}$ and angle variables $\{\theta\}$. The "photon" first moves for a random distance l_1 in a direction defined by angle ϕ_0, at which point it is scattered and turned through a random angle θ_1. The photon then moves a distance l_2 to the next point of interaction with the scattering medium, where, after being scattered through an angle θ_2, it moves a distance l_3, at which point it again changes direction. In this way, after n steps the x coordinate of the walker is given as

$$x = \sum_{i=1}^{n} l_i \cos(\phi_0 + \beta_i) \tag{1}$$

where β_i is defined as

$$\beta_i = \theta_1 + \cdots + \theta_{i-1} \tag{2}$$

Consequently, the root mean square distance traveled in an n-step random walk is given as $\langle x^2 \rangle^{1/2}$, where $\langle x^2 \rangle$ can be expressed, according to Eq. (1), as

$$\langle x^2 \rangle = \left\langle \sum_{i=1}^{n} x_i^2 + 2 \sum_{i=1}^{n} \sum_{j=1}^{i-1} x_i x_j \right\rangle \tag{3}$$

x_i being defined as

$$x_i = l_i \cos(\phi_0 + \beta_i) \tag{4}$$

Equation (3) can be rewritten as

$$\langle x^2 \rangle = \sum_{i=1}^{n} \langle x_i^2 \rangle + 2 \sum_{i=1}^{n} \sum_{j=1}^{i-1} \langle x_i x_j \rangle \tag{5}$$

Let $P_{sc}(l)\,dl$ represent the probability that a photon moves for a distance dl about l between collisions, and $p(\theta)\,d\theta$ be the probability that it turns into an angle $d\theta$ about θ. We assume that angles and step lengths are independent, and that the distribution of initial angles $p_0(\phi_0)$ is given simply as $p_0(\phi_0) = 1/(2\pi)$. Hence, the first term in Eq. (5) may be expressed as

$$\sum_{i=1}^{n} \langle x_i^2 \rangle = \frac{n\langle l^2 \rangle}{2} \tag{6}$$

where $\langle l^2 \rangle = \int_0^\infty l^2 P_{sc}(l)\,dl$. The cross terms $\langle x_i x_j \rangle$ may be evaluated according to

$$\begin{aligned}\langle x_i x_j \rangle &= \langle l_i \rangle \langle l_j \rangle \langle \cos(\phi_0 + \beta_i) \cos(\phi_0 + \beta_j) \rangle \\ &= \left[\int_0^\infty l P_{sc}(l)\,dl \right]^2 \cdot \int_{-\pi}^{\pi} p(\theta_{i-1})\,d\theta_{i-1} \\ &\quad \times \cdots \int_{-\pi}^{\pi} p(\theta_1)\,d\theta_1 \int_{-\pi}^{\pi} p_0(\phi_0) \cos(\phi_0 + \beta_i) \cos(\phi_0 + \beta_j)\,d\phi_0 \end{aligned} \tag{7}$$

The last integral may be written as

$$\begin{aligned}&\int_{-\pi}^{\pi} p_0(\phi_0) \cos(\phi_0 + \beta_i) \cos(\phi_0 + \beta_j)\,d\phi_0 \\ &\quad = \frac{1}{4\pi} \int_{-\pi}^{\pi} [\cos(\beta_i - \beta_j) + \cos(2\phi_0 + \beta_i + \beta_j)]\,d\phi_0\end{aligned}$$

and, from Eq. (2), we thus can express $\langle x_i x_j \rangle$ as

$$\langle x_i x_j \rangle = \frac{\langle l \rangle^2}{2} \int_{-\pi}^{\pi} p(\theta_{i-1})\,d\theta_{i-1} \cdots \int_{-\pi}^{\pi} p(\theta_1)\,\Re[e^{i(\theta_{i-1} + \cdots + \theta_j)}]\,d\theta_1 \tag{8}$$

For the problem at hand, it is reasonable to assume that $p(\theta)$ is an even function of θ, from which it follows that Eq. (8) may be expressed as

$$\langle x_i x_j \rangle = \frac{\langle l \rangle^2}{2} (p_1)^{i-j} \tag{9}$$

where p_1 is defined by

$$p_1 \equiv \int_{-\pi}^{\pi} \cos\theta\, p(\theta)\,d\theta \tag{10}$$

The sum of the off-diagonal terms appearing in Eq. (5) thus is

$$2\sum_{i=1}^{n}\sum_{j=1}^{i-1}\langle x_i x_j\rangle = \langle l\rangle^2 \frac{p_1}{1-p_1}\left(n-\frac{1-p_1^n}{1-p_1}\right) \tag{11}$$

and, by adding the quantities given in Eqs. (6) and (11), we find that the expression given by Eq. (3) becomes

$$\langle x^2\rangle = n\left(\frac{\langle l^2\rangle}{2}+\langle l\rangle^2\frac{p_1}{1-p_1}\right)-\langle l\rangle^2\frac{p_1(1-p_1^n)}{(1-p_1)^2} \tag{12}$$

From Eq. (12) we observe that, even in the limit of large n, the mean square distance traveled from the origin depends on the anisotropy factor p_1 in accordance with the specific character of the scattering process. That is, the functional relationship between $\langle x^2\rangle$ and p_1 implicitly depends on $P_{sc}(l)$. A related expression, for the special case of constant distances between scattering events, previously was derived by similar arguments.[16]

An extension to three dimensions is discussed in the Appendix, where we show that the three-dimensional analog of Eq. (12) is

$$\langle x^2\rangle = \frac{2}{3}n\left(\frac{\langle l^2\rangle}{2}+\langle l\rangle^2\frac{g}{1-g}\right)-\frac{2}{3}\langle l\rangle^2\frac{g(1-g^n)}{(1-g)^2} \tag{13}$$

where g is defined as [cf. Eq. (10)]

$$g \equiv \int_0^{\pi}\cos\theta\cdot p(\theta)\sin\theta\, d\theta \tag{14}$$

Here, in Eq. (14), θ is to be interpreted as the polar angle and, in contrast to the two-dimensional case, $p(\theta)$ is normalized such that $\int_0^{\pi} p(\theta)\sin\theta\, d\theta = 1$. Equation (13) is the basis for subsequent analysis. First, we consider the scattering free path to be distributed according to an exponential probability density

$$P_{sc}(l) = \lambda^{-1}e^{-l/\lambda} \tag{15}$$

where $\lambda = \Sigma_s^{-1}$ is the mean free path (Σ_s is the scattering cross section). In this case $\langle l^2\rangle = 2\lambda^2$ and $\langle l\rangle = \lambda$, so one finds from Eq. (13)

$$\langle x^2\rangle \sim \frac{2}{3}\frac{n\lambda^2}{1-g} \qquad \text{(exponential distribution; 3D)} \tag{16}$$

the two-dimensional analog of which was derived earlier in a different context.[17] For comparison, let us assume that the distances between steps

are fixed, so $P_{sc}(l)=\delta(l-\lambda)$ and $\langle l^2\rangle=\langle l\rangle^2=\lambda^2$. We now find that Eq. (13) yields a result which, except for a constant, has been derived previously for models of polymer chains,[16,18]

$$\langle x^2\rangle \sim \frac{n\lambda^2}{3}\frac{1+g}{1-g} \qquad \text{(constant scattering length; 3D)} \tag{17}$$

Lastly, suppose the scattering lengths are uniformly distributed over the range 0 to 2λ [i.e., $P_{sc}(l)=(2\lambda)^{-1}$ for $0\leqslant l\leqslant 2$; $P_{sc}(l)=0$, otherwise]. In this case $\langle l^2\rangle=4/3\lambda^2$, $\langle l\rangle=\lambda$, and we find

$$\langle x^2\rangle \sim \frac{2n\lambda^2}{9}\frac{2+g}{1-g} \qquad \text{(uniform distribution; 3D)} \tag{18}$$

Note that Eqs. (16)–(18) become indistinguishable for strong forward scattering, when $g\approx 1$.

3. PREDICTION OF SCALING RELATIONS FOR SURFACE PROFILES

A quantity of primary interest in this study is $\gamma(\rho)$, which is proportional to the number of walkers (or energy) returning to a surface at a distance ρ (in units of root mean square scattering length) from the point of insertion. A simple similarity transformation allows us to predict the g dependence of $\gamma(\rho)$ for any given scattering law $P_{sc}(l)$, once the pathlength distribution is specified or characterized.

Let us start with the following relationship between probability densities:

$$\gamma(\rho)=\int_0^\infty \mathscr{P}(\rho\,|\,n)\,P(n)\,dn \tag{19}$$

where $\mathscr{P}(\rho\,|\,n)$ is the conditional probability that a photon returns to the surface at point ρ, having made n collisions during its travel, and $P(n)$ is the path-length distribution for photons which return to the surface, the latter being evaluated without regard to the point where they are reemitted. We first assert that, in the quantity $\mathscr{P}(\rho\,|\,n)$, the variable ρ only appears in the combination $\rho^2/[nf(g)]$, where $f(g)$ is defined such that $\langle x^2\rangle=nf(g)$ [cf. Eq. (13)]; this observation {i.e., $\mathscr{P}(\rho\,|\,n)=\mathscr{P}(\rho^2/[nf(g)])$} is based on the derivation, appearing in ref. 11 for an isotropic scattering lattice, of an expression for the probability that a photon be reemitted at point ρ at the nth step. The latter quantity was obtained by making the assumption that the distribution of photon displacements on an infinite lattice, after an n-step random walk, is given as

$$P_n(\tilde{\mathbf{r}})=(3/2\pi n)^{3/2}\exp(-3\tilde{r}^2/2n)$$

where $\tilde{\mathbf{r}} = (x, y, z)$ is expressed in units of root mean square scattering length. This expression for $P_n(\tilde{r})$ is consistent with the notion that $\langle(\tilde{r})^2\rangle_{iso} = n$, i.e., that all distances scale as ρ^2/n. Following the analysis used in ref. 11 and using the expression given in Eq. (13), we construe that analogous results for anisotropic scattering can be obtained by making the substitution $\rho^2/n \to \rho^2/nf(g)$, where the specific form of $f(g)$ depends on the scattering-length distribution $P_{sc}(l)$. In terms of the distance variables appearing in Eqs. (16)–(18), the $\{P_n\}$ for isotropic scattering are $P_n(r) \sim \exp[-(3/4n)(r/\lambda)^2]$ (exponential distribution), $P_n(r) \sim \exp[-(3/2n)(r/\lambda)^2]$ (constant scattering length), and $P_n(r) \sim \exp[-(9/8n)(r/\lambda)^2]$ (uniform distribution).

From Monte Carlo calculations which are described in the next section (see Fig. 2), we empirically find that the dependence of $P(n)$ on the mean scattering angle can be conveniently expressed as

$$P(n) \leftrightarrow P\left(\left[\frac{1-g}{1+g}\right] \cdot n\right) \tag{20}$$

(Equation (20) seems to hold quite well, whatever the scattering length distribution, when the scaled variable $n^x = n[1-g]/[1-g]$ is small.) Thus, Eq. (19) can be written as

$$\gamma(\rho) \sim \int_0^\infty \mathscr{P}\left(\frac{\rho^2}{nf(g)}\right) P(nh(g))\, dn \tag{21}$$

where $h(g)$ is given as $h(g) \equiv (1-g)/(1+g)$. A simple coordinate transformation then yields

$$\gamma(\rho) \sim \int_0^\infty \mathscr{P}\left(\frac{\rho^2 h(g)}{\xi f(g)}\right) P(\xi)\, d\xi \tag{22}$$

so we see that $\gamma(\rho)$ is a functional of the reduced variable $\rho^* = \rho[h(g)/f(g)]^{1/2}$, i.e., $\gamma(\rho) = I([h(g)/f(g)]^{1/2}\rho)$. In accordance with Eqs. (16)–(18) and Eq. (20), we thus find the following scaling dependences for the surface emission probabilities:

$$\gamma(\rho) \leftrightarrow I([(1-g)/(1+g)^{1/2}]\,\rho)$$
(exponential distribution) (23a)

$$\gamma(\rho) \leftrightarrow I([(1-g)/(1+g)]\,\rho)$$
(constant scattering length) (23b)

$$\gamma(\rho) \leftrightarrow I(\sqrt{2}\,[(1-g)/(2+g)^{1/2}\,(1+g)^{1/2}]\,\rho)$$
(uniform distribution) (23c)

These predictions are in excellent agreement with results of simulations presented in Figs. 3 and 4, showing that the heuristic argument which leads to Eq. (22) indeed has merit.

4. SIMULATIONS

Monte Carlo simulations of the scattering of photons in an infinite medium were carried out, for various values of anisotropy coefficient g, for the three scattering-length probability densities which led to Eqs. (16)–(18). The mean scattering length was taken to be 1 for each case [$\lambda = 1$ in Eqs. (15)–(18)]. Except for the constant-step distribution, the path length between collisions was determined by comparing a randomly generated number between 0 and 1 with the cumulative probability distribution given by $P_{cum}(l) = \int_0^l P_{sc}(x)\,dx$. The latter was $P_{cum}(l) = 1 - \exp(-l)$ for an exponentially distributed scattering process [cf. Eq. (15)] and, for the uniform distribution, $P_{cum}(l) = l/2$ (for $0 \leqslant l \leqslant 2$). The random scattering length was taken to be that value of l for which $P_{cum}(l)$ equaled the selected random number.

The azimuthal angle ϕ was drawn randomly between values 0 and 2π. Unless otherwise indicated, the polar angle θ was determined from the cumulative probability distribution of the Henyey–Greenstein phase function,[19] which takes the form

$$F(\theta) = \frac{1-g^2}{2g}\left[\frac{1}{1-g} - \frac{1}{(1+g^2-2g\cos\theta)^{1/2}}\right], \quad 0 \leqslant \theta \leqslant \pi \tag{24}$$

In the case $g = \langle \cos\theta \rangle \to 0$, Eq. (24) takes the form

$$F(\theta)|_{g\to 0} = \frac{1-\cos\theta}{2} \tag{25}$$

which is the cumulative probability distribution of an isotropic diffusion process. The Henyey–Greenstein phase function, which empirically represents the scattering from a material which statistically scatters into a relatively broad range of angles including backscatter, often has been used in atmospheric studies as well as in investigations of biological tissue.

In the first of our calculations, the photons were isotropically launched in an initially random direction at $\mathbf{r} \equiv \{0, 0, 0\}$ and the coordinates computed for each step of the subsequent random walk. The displacement $\mathbf{R}$ from the origin and its projection x on a given axis were stored in a matrix for several thousand photons. The mean square displacements $\langle R^2 \rangle$ and $\langle x^2 \rangle$ then were computed for each step n. Three sets of data were obtained, one for each of the distributions studied above (exponential

distribution, constant step, and uniform distribution). Also, to observe the effect of the phase function on our results, several simulations were performed with a scattering angle density that is constant over a given cone of scattering angles. Such a distribution has no obvious physical analog, but it affords a good test of the universality of the theory. The cumulative probability distribution for a cone distribution is expressed as

$$F^*(\theta) = \begin{cases} (1-\cos\theta)/2(1-g) & \text{if } 0 \leqslant \theta \leqslant \cos^{-1}(2g-1) \\ 1 & \text{if } \cos^{-1}(2g-1) \leqslant \theta \leqslant \pi \end{cases} \tag{26}$$

In particular, when $g = 0.5$ the scattering is isotropic in the forward-directed half-plane, in which case Eq. (26) takes the form

$$F^*(\theta) = \begin{cases} 1-\cos\theta & \text{if } 0 \leqslant \theta \leqslant \pi/2 \\ 1 & \text{if } \pi/2 \leqslant \theta \leqslant \pi \end{cases} \tag{27}$$

In a different group of simulations, photons were inserted perpendicularly to a plane, at a point $\rho \equiv \{x, y\} = \{0, 0\}$. We wished to see how the presence of the plane might affect the results of counting procedures applied to the walks. Results were found to be in very good agreement with the analytical expressions given in Eqs. (16)–(18).

An example is shown in Fig. 1a, where the dependence of the mean square projected displacement $\langle x^2 \rangle$ is shown as a function of n for $g = 0.5$, for both the exponential and constant scattering-length distributions. In both instances, the curves associated with the Henyey–Greenstein and cone distributions are indistinguishable. Figure 1b shows the superpositions of mean square *surface* displacements, in this case as a function of total path length l_{Tot}, for an exponential scattering-length distribution for both reflecting and absorbing boundaries. Because the mean values of the scattering lengths have been chosen to be equal to one and the number of samples is large, the total path length on average equals the number of collisions. The slope of the curve in Fig. 1b is twice that predicted by Eq. (16) because the displacement in a plane is twice that of a projection along a line, i.e., $\langle \rho^2 \rangle = \langle x^2 \rangle + \langle y^2 \rangle$. For sufficiently large n, it mattered not if the photons entered with angles distributed uniformly over the entire half-space leading away from the surface (i.e., as a Lambertian source), rather than being injected perpendicularly to the boundary.

We continued to investigate the effects of a planar boundary by computing the length of the path that a photon traces before it reaches the surface after having been injected in a perpendicular direction. Representative results are shown in Fig. 2, where the path-length distribution $P(l_{Tot})$ is plotted as a function of $l_{Tot}(1-g)/(1+g)$. Figure 2a contains curves, for

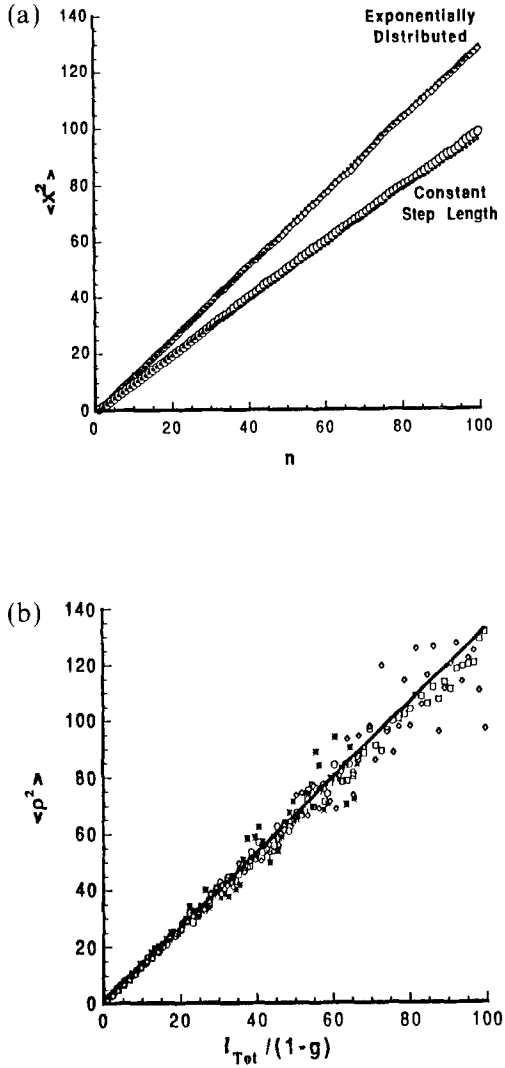

Fig. 1. Examples of results obtained from Monte Carlo simulations of random flight. (a) Mean-square displacement in an infinite medium $\langle x^2 \rangle$ as a function of the number of steps n for differing scattering angle distributions. Results for $g = 0.5$ of simulations with a Henyey–Greenstein distribution [Eq. (24)] and a uniform distribution in a cone [Eq. (27)] for the exponential and constant scattering-length distributions. (b) Mean-square surface displacement when photons exit a semi-infinite medium $\langle \rho^2 \rangle$ as a function of appropriate scaled path length for various values of g (+, $g = 0$; ◇, $g = 0.5$; △, $g = 0.8$; ○, $g = 0.9$) for exponential scattering. Here the scaling factor is $(1 - g)^{-1}$, in accordance with Eq. (16). The line has a slope of 4/3, as expected.

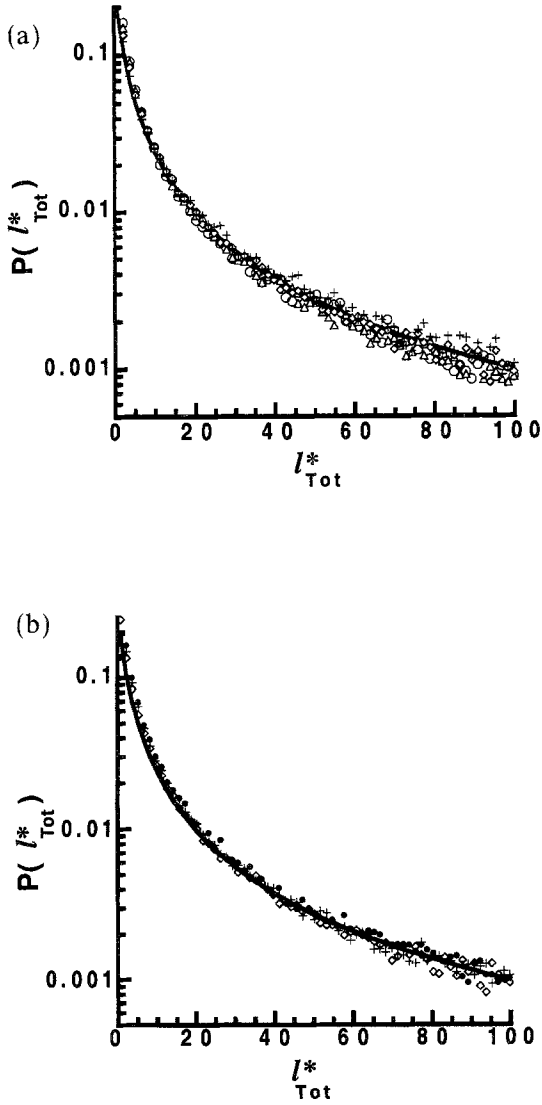

Fig. 2. Logarithm of the path-length distribution $P(l_{Tot})$ of photons returning to the surface after being inserted in a semi-infinite medium, plotted as a function of the scaled pathlength $l^*_{Tot} = l_{Tot}(1-g)/(1+g)$. (a) Distributions for exponential scattering lengths for various values of g (+, $g=0$; ◇, $g=0.5$; △, $g=0.8$; ○, $g=0.9$). (b) Distributions for $g=0.5$ for (◇) the exponential, (●) constant-scattering-length, and (+) uniform distributions. In both figures, the solid line is the expression $P(n) = Kn^{-1/2}(1-e^{-6/n})$, obtained by setting $\mu=0$ in Eq. (28) and integrating over ρ. (K here is a fitted constant which depends on the bin size of the Monte Carlo simulation.)

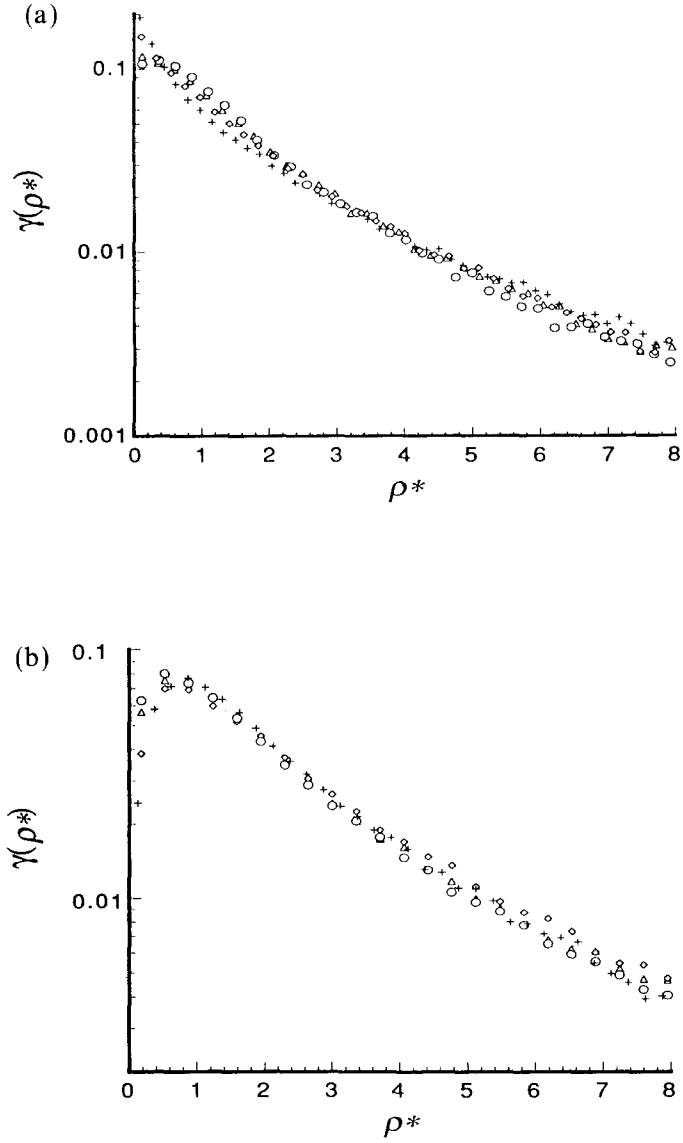

Fig. 3. Surface emission probability $\gamma(\rho)$ for different scattering-length distributions: (a) for exponentially distributed scattering, plotted as a function of the number of scaled root mean square scattering lengths, $\rho^* = \rho(1-g)/(1+g)^{1/2}$, for various values of g [cf. Eq. (23a)]; (b) for a constant scattering-length distribution, plotted as a function of $\rho^* = \rho(1-g)/(1+g)$ [cf. Eq. (23b)]; (c) for the uniform scattering-length distribution, plotted as a function of $\rho^* = \rho\sqrt{2}\,(1-g)/[(2+g)^{1/2}\,(1+g)^{1/2}]$ [cf. Eq. (23c)]. Key: +, $g=0$; ◇, $g=0.5$; △, $g=0.8$; ○, $g=0.9$.

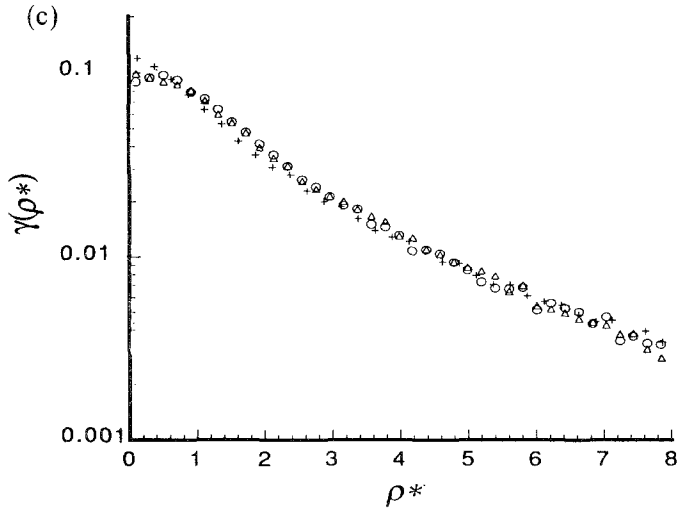

Fig. 3 (*continued*)

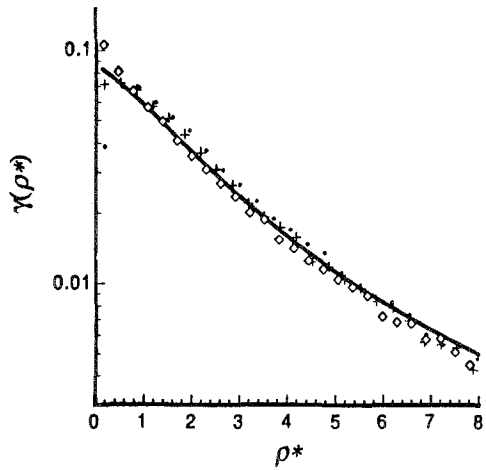

Fig. 4. Surface emission probability $\gamma(\rho)$ for $g = 0.5$. Each curve ($\diamond$, exponential distribution; $\bullet$, constant scattering-length; $+$, uniform distribution) is plotted as a function of ρ^* appropriate to the particular stochastic nature of the scattering process (see Fig. 3). The solid line is an expression obtained from Eq. (28) by integrating over n and multiplying by a constant to account for the bin size of the Monte Carlo simulation, i.e., $\gamma(\rho) \equiv 2\pi\rho \int_0^\infty \Gamma(\rho, n)\, dn \propto [1 - \rho/(\rho^2+4)^{1/2}]$.

different values of g, for the exponential scattering-length distribution. Figure 2b shows results, for $g = 0.5$, for each of the scattering-length distributions discussed previously (exponential distribution, constant step, and uniform distribution). We note that the curves superimpose very well, indicating that the distribution of total path length can be scaled by a universal function of g. On average, the total path length is proportional to the number of collisions, i.e., $l_{Tot} \sim n\langle l \rangle$, so the results shown in Fig. 2 lead us to infer the relationship expressed in Eq. (20). The solid lines are obtained from a previously developed theory of migration in an isotropic scattering medium[11] (see figure caption).

The same simulated data were used to calculate the diffuse surface reflectance $P(\rho)$. Results are shown in Figs. 3 and 4. Note that the predictions of Eqs. (23) are very well substantiated, implying that the scaling relation given in Eq. (22) probably is generally valid. In particular, the patterns of backscattered intensity at small values of ρ^* can be superimposed if scaled by the factors given in Eqs. (23a)–(23c).

5. DISCUSSION

The calculations described in the foregoing sections were motivated by an ongoing interest in developing and refining theories of tissue optics.[11–14] As already mentioned, the effects of tissue absorption have not been considered; however, the scaling information obtained in this work forms the basis of a similar analysis in which photon absorption is taken into account.[15] Although the studies herein described are applicable to a number of stochastic behaviors, they specifically lead to the following inferences regarding the migration of photons in a multiply scattering medium: (1) the signature encompassed in the pattern of diffuse surface reflectance (i.e., surface emission density) is degenerate, in that different combinations of scattering-length distributions and angular scattering cross section yield nearly the same surface profiles; (2) different materials, characterized by different scattering-length distributions, give rise to dissimilar scaling rules, but the variations will be unimportant if the scattering is strongly peaked in the forward direction [see, e.g., Eqs. (23)]; (3) if done properly, angularly anisotropic scattering processes can be described by an equivalent isotropic transport theory; (4) there exists an empirical scaling relation for short path lengths, associated with anisotropic scattering, which may be a universal function of g and the bulk scattering cross section Σ_s (Fig. 2).

The scaling of absorption coefficients is fully discussed in the companion paper.[15] If, as indicated in the present work, in equivalent isotropic theories the path lengths are to be scaled by the factor

$(1-g)/(1+g)$, then the absorption coefficients should be multiplied by its inverse, $(1+g)/(1-g)$. Additionally, because an exponential distribution is a close approximation of the probabilistic character of the photon scattering that takes place in random media, Eq. (23a) and Fig. 3a suggest that lengths should be scaled as $\rho^* = (r/\sqrt{2})\,\Sigma_s(1-g)/(1+g)^{1/2}$. The fact that such scaling relationships exist explains why analytic expressions derived for isotropic scattering media work so well in fitting results of photon time-of-flight measurements of biological tissues.[14,20]

These inferences can be used to extend the theories that we developed[11] previously to describe photon migration in turbid media. It had long been assumed that the earlier results could be reexpressed in terms of appropriate transport-corrected scattering and absorption cross sections, and we now have explicit expressions for those parameters. Transformation of analytical expressions is well illustrated by considering the joint probability $\Gamma(\rho, n)$ that a photon (or random walker) returns to the surface of a semi-infinite medium at point ρ, after the nth sep. Based on our earlier photon migration model, which is related to a discrete step model of transport, this quantity is given by

$$\Gamma(\rho, n) = \frac{\sqrt{3}}{2}(2\pi n)^{-3/2}\,(1 - e^{-6\rho_0^2/n})\,e^{-3\rho^2/2n}e^{-\mu n} \tag{28}$$

where μ is the absorption per unit step and ρ_0 is the lattice point where the initial scattering occurs, here taken to be $\rho_0 = 1$. In order to express Eq. (28) in terms of *real* variables (d, t), where d is the displacement along the surface, we first must make the substitutions $(\rho, n) \to (\rho^*, n^*)$, where

$$\rho \to \rho^* = \frac{d}{\sqrt{2}}\frac{1-g}{(1+g)^{1/2}}\Sigma_s \tag{29}$$

and

$$n \to n^* = n\frac{1-g}{1+g} \tag{30}$$

Further, upon noting that $n\langle l\rangle = n\Sigma_s^{-1} = c_T t$, where c_T is the speed of light in the medium, we write

$$n^* = \frac{1-g}{1+g}\Sigma_s c_T t \tag{31}$$

With these substitutions, Eq. (28) becomes

$$\Gamma(d, t) \propto t^{-3/2}(1-\exp\{-[6(1+g)]/[(1-g)\,\Sigma_s c_T t]\}) \times \exp\{-[3d^2(1-g)\,\Sigma_s]/4c_T t\}\exp(-\Sigma_a c_T t) \tag{32}$$

Note that the dependence of $\langle d^2\rangle$ here is in agreement with the behavior show in Fig. 1b.

Except at short times, this expression is identical to that obtained by solving the "transport-corrected" optical diffusion equation.[20] The latter has the same form as the diffusion equation for isotropic angular scattering, except that the scattering cross section Σ_s is replaced by $\Sigma_s' = (1-g)\,\Sigma_s$. However, such a simple fix-up of theories of isotropic scattering may not always be appropriate, as the simple substitution $\Sigma_s \to (1-g)\,\Sigma_s$ implies a dependence on the scaled variable $d^* = (1-g)^{1/2}\,d$, which would be at variance with the simulations shown in Fig. 3a. Moreover, integration of Eq. (32) over ρ yields

$$\Gamma(t) \propto t^{-1/2}[1-\exp(-6/\tilde{\Sigma}_s c_T t)]\exp(-\Sigma_a c_T t) \tag{33}$$

where $\tilde{\Sigma}_s = [(1-g)/(1+g)]\,\Sigma_s$. Clearly, in this case it would be incorrect to replace the cross section by the usual "transport-corrected" quantity.

Quasielastic light scattering experiments on multiply scattering media,[21] in which the number of photon collisions with colloidal particles can be measured, may be used to test these scaling relations in a quantitative fashion. We note, though, that at large distances or long times, experimental results might be indistinguishable from those which would be predicted by certain other sets of consistent scaling relations. In particular, for an exponential scattering length distribution, Eq. (22) is satisfied when the variables ρ^* and n^* both scale as $(1-g)$, i.e., $\{\gamma(\rho) \leftrightarrow I([1-g]\rho);\ P(n) \leftrightarrow P([1-g]n)\}$ (cf., Eqs. (20) and (23a)). Although simulations indicate that when short pathlengths are considered the latter scaling does not provide results as satisfactory as those shown in Figs. (2) and (3a), excellent superpositions for longer pathlength random walks indeed are obtained with such $(1-g)$ scaling. On the other hand, when constant scattering length random walks are studied, one finds that $(1-g)/(1+g)$ scaling works extremely well for both $\gamma(\rho)$ and $P(n)$, over the entire range of pathlengths (cf. Eq. (17)).

Finally, we remark that the above theory applies to photon migration in turbid media when phase information can be ignored. Due to the coherence properties of laser light, in special circumstances enhanced backscattered intensities can be discerned over a very small angle near the point where light is inserted into a random medium.[22,23] Such components,

which are not accounted for in the present theory, are ascribed to localization effects. However, they constitute a vanishingly small portion of the total diffuse reflected intensity and therefore are of little importance when light is collected over a large solid angle.

APPENDIX: PROOF OF EQ. (13)

We now provide a short proof of the expression for the mean square distance traveled by a walker in an infinite, *3-dimensional*, medium. In analogy with Eq. (5), we have $\langle x^2 \rangle = \frac{1}{3}\langle L^2 \rangle$, where $\boldsymbol{L}$ is the sum of the vectors describing the individual steps of the walk, $\boldsymbol{L} = \sum_{j=1}^{n} \boldsymbol{l}_j$. Hence, $\langle L^2 \rangle$ is given as

$$\langle L^2 \rangle = \sum_{i=1}^{n} \langle l_i^2 \rangle + 2 \sum_{i=1}^{n} \sum_{j=1}^{i-1} \langle \boldsymbol{l}_i \cdot \boldsymbol{l}_j \rangle \tag{A.1}$$

Because the individual steps are assumed to be identically distributed, the first term in the equation can be written as [cf. Eq. (6)]

$$\sum_{i=1}^{n} \langle l_i^2 \rangle = n \langle l^2 \rangle \tag{A.2}$$

To compute the second term in this expansion, let us represent each vector step in the form $\boldsymbol{l}_j = l_j \boldsymbol{U}_j$, where $\boldsymbol{U}_j$ is a unit vector in the direction of $\boldsymbol{l}_j$, and let us denote the Cartesian coordinates $\{\boldsymbol{U}_j, \boldsymbol{V}_j, \boldsymbol{W}_j\} \equiv \mathbf{R}_j$ to be the reference frame for the jth step.[24] ($\boldsymbol{V}_j$ and $\boldsymbol{W}_j$ are mutually perpendicular vectors, both perpendicular to $\boldsymbol{U}_j$.) The vector $\boldsymbol{l}_{j+1}$ then can be represented in terms of the coordinates $\mathbf{R}_j$ as $\boldsymbol{l}_{j+1} = l_{j+1} \boldsymbol{U}_{j+1}$, where $\boldsymbol{U}_{j+1}$ is expressed as the product of a 3×3 matrix $\bar{X}_{j+1}$ and a 1×3 column matrix $\bar{d}$ as $\boldsymbol{U}_{j+1} = \bar{X}_{j+1} \cdot \bar{d}$, the latter being defined as[24,25]

$$\bar{X}_{j+1} = \begin{pmatrix} \cos\theta_{j+1} & -\sin\theta_{j+1} & 0 \\ \sin\theta_{j+1}\cos\phi_{j+1} & \cos\theta_{j+1}\cos\phi_{j+1} & -\sin\phi_{j+1} \\ \sin\theta_{j+1}\sin\phi_{j+1} & \cos\theta_{j+1}\sin\phi_{j+1} & \cos\phi_{j+1} \end{pmatrix} \tag{A.3}$$

and

$$\bar{d} = \begin{pmatrix} 1 \\ 0 \\ 0 \end{pmatrix} \tag{A.4}$$

Here θ_{j+1} and ϕ_{j+1} represent, respectively, the polar and azimuthal angles of $\boldsymbol{U}_{j+1}$ taken with respect to the coordinate system $\mathbf{R}_j$.

Note that the first component of $\boldsymbol{l}_{j+1}$ in the reference frame $\mathbf{R}_j$ is in the

direction of $\boldsymbol{U}_j$. By extension, the vector $\boldsymbol{l}_i$, for $i > j$, can be represented in $\mathbf{R}_j$ as

$$\boldsymbol{l}_i = l_i \boldsymbol{U}_i = l_i \left(\prod_{m=j+1}^{i} \bar{X}_m \right) \cdot \bar{d} \equiv l_i \bar{Y}_{i-j} \cdot \bar{d} \tag{A.5}$$

the first component of which will be in the direction of $\boldsymbol{U}_j$. (The matrix product is obtained by first multiplying $\bar{X}_{j+1}$ by $\bar{X}_{j+2}$, then multiplying by $\bar{X}_{j+3}$, etc.) Hence, $\boldsymbol{l}_j \cdot \boldsymbol{l}_i$ can be obtained as

$$\boldsymbol{l}_j \cdot \boldsymbol{l}_i = (l_j l_i) \times \text{first component of } \bar{Y}_{i-j} \cdot \bar{d}$$

and the expectation $\langle \boldsymbol{l}_j \cdot \boldsymbol{l}_i \rangle$ may be expressed as

$$\langle \boldsymbol{l}_j \cdot \boldsymbol{l}_i \rangle = \langle l_j \rangle \langle l_i \rangle \times \langle \{\text{first component of } \bar{Y}_{i-j} \cdot \bar{d}\} \rangle$$

Recognizing that the components of the matrices $\{\bar{X}_m\}$ are independent, we immediately find, because $\langle \cos \phi \rangle = \langle \sin \phi \rangle = 0$ (uniform distribution), that $\langle \bar{Y}_{i-j} \rangle$ can be expressed as $\langle \bar{Y}_{i-j} \rangle = \langle \bar{X} \rangle^{i-j}$, where $\langle \bar{X} \rangle$ is given as[24]

$$\langle \bar{X} \rangle = \begin{pmatrix} \langle \cos \theta \rangle & -\langle \sin \theta \rangle & 0 \\ 0 & 0 & 0 \\ 0 & 0 & 0 \end{pmatrix} \tag{A.6}$$

Consequently, one finds[24]

$$\langle \boldsymbol{l}_j \cdot \boldsymbol{l}_i \rangle = \langle l_j \rangle \langle l_i \rangle \langle \cos \theta \rangle^{i-j} \tag{A.7}$$

and Eq. (13) follows after noting that the double sum in Eq. (A.1) can be evaluated according to a summation similar to that given in Eq. (11).

REFERENCES

1. F. G. Fernald, *Appl. Opt.* **23**:652 (1984).
2. J. D. Klett, *Appl. Opt.* **24**:1638 (1985).
3. H. R. Gordon, R. C. Smith, and J. R. V. Zaneveld, *Proc. SPIE* **489**:2 (1984).
4. M. A. Blizard, *Proc. SPIE* **637**:2 (1986).
5. B. White, P. Sheng, M. Postel, and G. Papanicolaou, *Phys. Rev. Lett.* **63**:2228 (1989).
6. J. Chang and Y. C. Yortsos, *SPE Form. Eval.* **1990** (March): 31; R. A. Beier, SPE paper 20582, presented at the 65th Annual Technical Conference of the Society of Petroleum Engineers, New Orleans, Louisiana (1990).
7. M. Stern, *Nature* **254**:56 (1975).
8. R. Bonner and R. Nossal, *Appl. Opt.* **20**:2097 (1981); R. Bonner and R. Nossal, in *Laser-Doppler Blood Flowmetry*, A. P. Shepherd, Jr., and P. Å. Öberg, eds. (Kluwer Academic, Boston, 1990), Chapter 2.

9. D. T. Delpy, M. Cope, P. van de Zee, S. Arridge, S. Wray, and J. Wyatt, *Phys. Med. Biol.* **33**:1433 (1988); B. Chance, J. S. Leigh, H. Miyake, D. S. Smith, S. Nioka, R. Greenfeld, M. Finander, K. Kaufmann, W. Levy, M. Yound, P. Cohen, H. Yoshioka, and R. Boretsky, *Proc. Natl. Acad. Sci. USA* **85**:4971 (1988).
10. J. M. Schmitt, G. X. Zhou, E. C. Walker, and R. T. Wall, *J. Opt. Soc. Am. A* **14**:2141 (1990).
11. R. Bonner, R. Nossal, S. Havlin, and G. H. Weiss, *J. Opt. Soc. Am. A* **4**:423 (1987).
12. R. Nossal, J. Kiefer, G. H. Weiss, R. Bonner, H. Taitelbaum, and S. Havlin, *Appl. Opt.* **27**:3382 (1988); G. H. Weiss, R. Nossal, and R. F. Bonner, *J. Mod. Opt.* **36**:349 (1989).
13. R. Nossal, R. F. Bonner, and G. H. Weiss, *Appl. Opt.* **28**:2238 (1989).
14. R. Nossal and R. F. Bonner, *SPIE Proc.* **1431**:21 (1991).
15. A. H. Gandjbakhche, R. Nossal, and R. F. Bonner, *Appl. Opt.*, submitted.
16. J. Frenkel, *Kinetic Theory of Liquids* (Dover, New York, 1955), p. 464.
17. R. Nossal and G. H. Weiss, *J. Stat. Phys.* **10**:245 (1974).
18. W. J. Taylor, *J. Chem. Phys.* **16**:257 (1948).
19. L. G. Henyey and J. L. Greenstein, *Ap. J.* **93**:70 (1941).
20. M. Patterson, B. Chance, and B. C. Wilson, *Appl. Opt.* **28**:2331 (1989).
21. R. Nossal and J. M. Schmitt, *Proc. SPIE* **1430**:37 (1991).
22. Y. Kuga and A. Ishimaru, *J. Opt. Soc. Am. A* **1**:831 (1984).
23. M. P. van Albada and A. Lagendijk, *Phys. Rev. Lett.* **55**:2692 (1985); P. E. Wolf and G. Maret, *Phys. Rev. Lett.* **55**:2696 (1985).
24. M. Kac, *Probability and Related Topics in Physical Sciences* (Interscience, New York, 1959), p. 35.
25. A. H. Gandjbakhche, Thesis, Université de Paris VII (1989); A. H. Gandjbakhche, P. Mills, and P. Snabre, *Appl. Opt.*, submitted.